

Newtonized Orthogonal Matching Pursuit for Line Spectrum Estimation with Multiple Measurement Vectors

Lin Han, Jiang Zhu, Rick S. Blum and Zhiwei Xu

Abstract

A Newtonized orthogonal matching pursuit (NOMP) algorithm is proposed to estimate continuous frequencies and amplitudes of a mixture of sinusoids with multiple measurement vectors (MMVs). The proposed algorithm includes two key steps: Detecting a new sinusoid on an oversampled discrete Fourier transform (DFT) grid and refining the parameters of already detected sinusoids to avoid the problem of basis mismatch. We provide a stopping criterion based on the overestimating probability of the model order. In addition, the convergence of the proposed algorithm is also proved. Finally, numerical results are conducted to investigate the effectiveness of the proposed algorithm when compared against the state-of-the-art algorithms in terms of frequency estimation accuracy and run time.

Index terms— Orthogonal matching pursuit, frequency estimation, line spectrum, Newton refinement, multiple measurement vectors

I. INTRODUCTION

One of the classical problems in digital communication and radar processing applications is to estimate continuous-valued frequencies of sinusoids in additive white Gaussian noise (AWGN) environments from a small number of measurements [1, 2]. On the one hand, several classical subspace methods have been proposed to perform the frequency estimation, such as MUSIC and ESPRIT [3, 4], which exploit the autocorrelation matrix's low-rank structure to estimate the underlying signal subspace. As the signal-to-noise ratio (SNR) decreases, the performance of these two algorithms for estimating closely spaced frequencies will degrade [5]. On the other hand, a variety of methods based on sparse representation and compressed sensing (CS) have also been proposed to estimate frequencies for multiple sinusoids [6, 7]. Basically, the estimation problem can be transformed to that of seeking a sparse approximation of the multiple sinusoids by referring to an infinite-dimensional dictionary. In fact, if all the frequencies lie on the discrete Fourier transform (DFT) grid, it can be shown that the signal can exactly be recovered by utilising convex optimization from randomly selected samples with high probability [8].

However, there exists a major grid mismatch problem induced by the fact that the measurements are sparsely represented under a finite discrete dictionary, which badly deteriorates the performance of various reconstruction algorithms. In fact, one has to make a reasonable tradeoff between the oversampling rate and the computational cost when implementing sparse methods. This unavoidable grid mismatch problem is studied in [9–11] in detail. Moreover, sparse reconstruction methods usually entail one or more parameters which in fact are not necessarily known, such as the number of the sinusoids, the regularization parameters, the variance of the noise and so on. Recently, the semiparametric iterative covariance-based estimation (SPICE) algorithm [12–14] has been proposed to alleviate the drawbacks of the discretization operation to a great extent, which uses the covariance fitting criterion from a statistical perspective and no user-parameters are required.

A. Related work

An exact discretization-free method, called the sparse and parametric approach (SPA) for uniform and sparse linear arrays, is proposed in [15]. This algorithm utilises the advantage of multiple measurement vectors (MMVs) to perform line spectrum estimation by solving a semidefinite programming problem. In [16], two approaches are developed to solve the problem of line spectrum denoising and estimation, which estimate an ensemble of spectrally-sparse signals composed of the same set of continuous-valued frequencies from MMVs. The iterative reweighted approach (IRA) is proposed to deal with both single measurement vector (SMV) and MMV settings [17], where all the frequencies are updated in parallel with good initial frequency estimates.

The most related work is the Newtonized orthogonal matching pursuit (NOMP) algorithm proposed in [18] considered for SMV settings. The authors provided a constant false alarm rate (CFAR) based on the stopping criterion, a detailed convergence analysis result and a comprehensive comparison with state-of-the-art algorithms. The work presented here has focused on the formulation of the NOMP algorithm with MMVs to estimate frequencies over the continuum, which is especially important in array signal processing fields. We not only extend the NOMP to MMVs scenarios, but also characterize convergence and provide a stopping criterion based on the given probability of overestimating the model order.

B. Contributions

The main contributions are summarized as follows:

- We extend the NOMP algorithm to deal with line spectrum estimation in the MMVs setting. Similar to the NOMP [18], our proposed algorithm avoids the basis mismatch problem by using a Newton refinement step as feedback to improve the estimation of already detected sinusoids. Besides this, the model order K is not needed in advance during estimation of frequencies of the sinusoids in the mixture, and a stopping criterion based on probability is provided.
- We analyze the convergence of the NOMP algorithm in MMVs settings by using the theory of dual norms. Specifically, we provide an upper bound on the number of iterations required by the NOMP method with MMVs to meet the provided stopping criterion and also obtain a bound on the convergence rate.
- By implementing numerical simulations to compare the estimation performance of various algorithms against the Cramér-Rao bound (CRB) in different scenarios, we show that the algorithm can achieve a near-optimal performance in terms of estimation accuracy.
- We analyze the computation time in four scenarios conducted in the simulation section. It can be shown that the proposed algorithm is faster than SPA, IRA and basis pursuit de-noising (BPDN), but slower than the classical MUSIC method.

Outline: In Section II, we set up our problem model. We propose our algorithm in Section III. In Section IV, we present the stopping criterion based on the probability of overestimating the model order, along with an analytical expression of the miss probability of detecting the sinusoids. We present the analysis of convergence in Section V. In Section VI, we conduct numerical experiments to compare the estimation accuracy of the NOMP with MMVs against the state-of-the-art methods. Section VII concludes the paper. *Notation:* We use $(\cdot)^H$, $(\cdot)^T$ and $(\cdot)^*$ to denote the conjugate transpose, transpose and conjugate operator respectively. \mathcal{CN} denotes the complex Gaussian distribution. The Frobenius norm, the real part of the complex number a and the trace operator are denoted by $\|\cdot\|_F^2$, $\Re\{a\}$ and $\text{tr}\{\cdot\}$ respectively. $[a]$ denotes the greatest integer that is less than or equal to a . \otimes is the Kronecker product operator.

II. PROBLEM SETUP

In an MMV model, we consider a line spectrum estimation scenario with N sensors and T snapshots collecting measurements of K distinct frequency components. The measurements at the array output can be expressed as

$$\mathbf{Y} = \Phi \mathbf{A} \mathbf{X} + \mathbf{Z}, \quad (1)$$

where the l th column of \mathbf{A} is defined as

$$\mathbf{a}(\omega_l) \triangleq \frac{1}{\sqrt{N}} \left[1, e^{j\omega_l}, \dots, e^{j(N-1)\omega_l} \right]^T, \quad (2)$$

where $\mathbf{Y} \in \mathbb{C}^{M \times T}$ is the noisy measurement collected by all N sensors and T snapshots, $\Phi \in \mathbb{C}^{M \times N}$ is the known compression matrix and $\mathbf{A} = [\mathbf{a}(\omega_1), \dots, \mathbf{a}(\omega_K)] \in \mathbb{C}^{N \times K}$. Each ω_l is continuous-valued in $[0, 2\pi)$. Furthermore, z_{ij} is independent and identically distributed (i.i.d.) Gaussian random variable and follows $z_{ij} \sim \mathcal{CN}(0, \sigma^2)$. $\mathbf{X} = [\mathbf{x}_1, \dots, \mathbf{x}_T] \in \mathbb{C}^{K \times T}$ contains all the sinusoid amplitudes x_{ij} for each snapshot. The uniform linear array (ULA) scenario for DOA can also be formulated as model (1) [15].

Before moving forward we make the following assumptions on the statistics of the sources and noises:

- 1) Sources are uncorrelated.
- 2) Sources and noises are independent.
- 3) Noises at different sensors are uncorrelated.

III. ALGORITHM

We first look into the estimation problem of a single sinusoid in the compressed scenarios, and then generalize the results to a mixture of sinusoids.

A. Single frequency

In this scenario, the model (1) simplifies to

$$\mathbf{Y} = \Phi \mathbf{a} \mathbf{x}^T + \mathbf{Z}, \quad (3)$$

where $\Phi \in \mathbb{C}^{M \times N}$, $\mathbf{x} = [x_1, \dots, x_T]^T \in \mathbb{C}^{T \times 1}$, and $\mathbf{a} = [1, e^{j\omega}, \dots, e^{j(N-1)\omega}]^T / \sqrt{N}$.

The Maximum Likelihood (ML) estimate of the amplitudes \mathbf{x} and frequency ω can be calculated by minimizing the residual power $\|\mathbf{Y} - \Phi \mathbf{a} \mathbf{x}^T\|_F^2$, which is equal to maximizing the function

$$S(\mathbf{x}, \omega) = 2\text{tr}\{\Re\{\mathbf{Y}^H \mathbf{a}_\Phi \mathbf{x}^T\}\} - \|\mathbf{a}_\Phi \mathbf{x}^T\|_F^2, \quad (4)$$

where $\mathbf{a}_\Phi = \Phi \mathbf{a}$.

It's difficult to directly optimize $S(\mathbf{x}, w)$ over all amplitudes and frequency. As a result, a two stage procedure is adopted: (1) Detection stage, in which a coarse estimate of ω is found by restricting it to a discrete set, (2) Refinement stage, where we iteratively refine the estimates of amplitudes and frequency of detected sinusoids. By using the least squares method procedure, we can then obtain the expression of \mathbf{x}^T that maximizes $S(\mathbf{x}, \omega)$ for any given ω , i.e., by setting $\partial S(\mathbf{x}, \omega)/\partial \mathbf{x}^* = \mathbf{a}_\Phi^H \mathbf{Y} - \mathbf{a}_\Phi^H \mathbf{a}_\Phi \mathbf{x}^T = 0$ [19], we obtain

$$\mathbf{x}^T = (\mathbf{a}_\Phi^H \mathbf{a}_\Phi)^{-1} \mathbf{a}_\Phi^H \mathbf{Y} = \mathbf{a}_\Phi^H \mathbf{Y} / \|\mathbf{a}_\Phi\|_2^2. \quad (5)$$

Substituting \mathbf{x}^T in $S(\mathbf{x}, w)$ allows us to find the ML estimate of ω , which is the solution to the following optimization problem:

$$\hat{\omega} = \underset{\omega}{\operatorname{argmax}} \mathbf{G}_Y(\omega), \quad (6)$$

where

$$\mathbf{G}_Y(\omega) = \|\mathbf{Y}^H \mathbf{a}_\Phi\|_2^2 / \|\mathbf{a}_\Phi\|_2^2. \quad (7)$$

Detection: By restricting ω to a finite discrete set denoted by $\Omega \triangleq \{k(2\pi/\gamma N) : k = 0, 1, \dots, (\gamma N - 1)\}$, where γ is the oversampling factor relative to the DFT grid, we can obtain a coarse estimate of ω . We treat the $\omega_c \in \Omega$ that maximizes the cost function (7) as the output of this stage, and the corresponding \mathbf{x}^T vector estimate is $\mathbf{a}_\Phi^H(\omega_c) \mathbf{Y} / \|\mathbf{a}_\Phi(\omega_c)\|_2^2$.

Refinement: Let $(\hat{\mathbf{x}}, \hat{\omega})$ denote the current estimate, then the Newton procedure for frequency refinement can be denoted as

$$\hat{\omega}' = \hat{\omega} - \dot{\mathbf{G}}_Y(\hat{\omega}) / \ddot{\mathbf{G}}_Y(\hat{\omega}), \quad (8)$$

where

$$\dot{\mathbf{G}}_Y(\hat{\omega}) = \operatorname{tr} \left\{ \mathcal{R} \left\{ \mathbf{Y}^H \left(\frac{d\mathbf{a}_\Phi}{d\omega} \mathbf{a}_\Phi^H + \mathbf{a}_\Phi \frac{d\mathbf{a}_\Phi^H}{d\omega} \right) \mathbf{Y} / \|\mathbf{a}_\Phi\|_2^2 - \mathbf{Y}^H \mathbf{a}_\Phi \mathbf{a}_\Phi^H \mathbf{Y} \left(\frac{d\mathbf{a}_\Phi}{d\omega} \mathbf{a}_\Phi + \mathbf{a}_\Phi \frac{d\mathbf{a}_\Phi^H}{d\omega} \right) / (\|\mathbf{a}_\Phi\|_2^2)^2 \right\} \right\}, \quad (9)$$

$$\ddot{\mathbf{G}}_Y(\hat{\omega}) =$$

$$\operatorname{tr} \left\{ \mathcal{R} \left\{ \frac{\mathbf{Y}^H}{\|\mathbf{a}_\Phi\|_2^2} \left(\frac{d^2 \mathbf{a}_\Phi}{d\omega^2} \mathbf{a}_\Phi^H + 2 \frac{d\mathbf{a}_\Phi}{d\omega} \frac{d\mathbf{a}_\Phi^H}{d\omega} + \mathbf{a}_\Phi \left(\frac{d^2 \mathbf{a}_\Phi}{d\omega^2} \right)^H \right) \mathbf{Y} - \frac{2\mathbf{Y}^H}{(\|\mathbf{a}_\Phi\|_2^2)^2} \left(\frac{d\mathbf{a}_\Phi}{d\omega} \mathbf{a}_\Phi^H + \mathbf{a}_\Phi \frac{d\mathbf{a}_\Phi^H}{d\omega} \right) \mathbf{Y} \left(\frac{d\mathbf{a}_\Phi^H}{d\omega} \mathbf{a}_\Phi + \mathbf{a}_\Phi \frac{d\mathbf{a}_\Phi}{d\omega} \right) - \frac{\mathbf{Y}^H \mathbf{a}_\Phi \mathbf{a}_\Phi^H \mathbf{Y}}{(\|\mathbf{a}_\Phi\|_2^2)^2} \left(\left(\frac{d^2 \mathbf{a}_\Phi}{d\omega^2} \right)^H \mathbf{a}_\Phi + 2 \frac{d\mathbf{a}_\Phi^H}{d\omega} \frac{d\mathbf{a}_\Phi}{d\omega} + \mathbf{a}_\Phi^H \frac{d^2 \mathbf{a}_\Phi}{d\omega^2} \right) + \frac{2\mathbf{Y}^H \mathbf{a}_\Phi \mathbf{a}_\Phi^H \mathbf{Y}}{(\|\mathbf{a}_\Phi\|_2^2)^3} \left(\frac{d\mathbf{a}_\Phi^H}{d\omega} \mathbf{a}_\Phi + \mathbf{a}_\Phi \frac{d\mathbf{a}_\Phi}{d\omega} \right)^2 \right\} \right\}. \quad (10)$$

We maximize $\mathbf{G}_Y(\omega)$ by employing the update rule (8) on the condition that the function is locally concave.

B. Multiple frequency

Assume that we have already detected k sinusoids, and let $P = \{(\mathbf{x}_l, \omega_l), l = 1, \dots, L\}$ denote the set of estimates of the detected sinusoids. The residual measurement corresponding to this estimate can be given by

$$\mathbf{Y}_r(P) = \mathbf{Y} - \sum_{l=1}^L \mathbf{a}_\Phi(\omega_l) \mathbf{x}_l^T \quad (11)$$

The method of estimating multiple frequencies proceeds by employing the single sinusoid procedure to perform Newtonized coordinate descent on the residual energy $\|\mathbf{Y}_r(P)\|_F^2$. One step of this coordinate descent involves adjusting all ω_l . The procedure to refine the l th sinusoid is as follows: $\mathbf{Y}_r(P \setminus \{\mathbf{x}_l, \omega_l\})$ now is referred to as the measurement \mathbf{Y} and the single frequency update step is utilised to refine (\mathbf{x}_l, ω_l) .

Refinement Acceptance Condition (RAC): This refinement step is accepted when it results in a strict improvement in $G_{\mathbf{Y}_r(P \setminus \{\mathbf{x}_l, \omega_l\})}(\omega)$, namely, $G_{\mathbf{Y}_r}(\hat{\omega}') > G_{\mathbf{Y}_r}(\hat{\omega})$. By doing this, we can make sure that the adopted refinement must decrease the overall residual energy.

In summary, firstly, we detect a frequency $\hat{\omega}$ over the discrete set Ω by maximizing the cost function (7). Then we use the knowledge of the first-order and second-order derivative of the cost function to refine the estimate of $\hat{\omega}$. Next, we use the information of all the other previously detected sinusoids to further improve the estimation performance of every previously detected sinusoid one at a time. This step is crucial for the convergence and accuracy of the algorithm. Finally, we update \mathbf{x} by least squares methods. The whole algorithm is summarized in Algorithm 1.

Algorithm 1 Multi snapshot NOMP.

- 1: **Procedure** EXTRACTSPECTRUM (\mathbf{Y}, τ) :
 - 2: $m \leftarrow 0, P_0 = \{\}$
 - 3: **while** $\max_{\omega \in \text{DFT}} G_{\mathbf{Y}_r(P_m)}(\omega) > \tau$ **do**
 - 4: $m \leftarrow m + 1$
 - 5: **IDENTIFY**
 $\hat{\omega} = \arg \max_{\omega \in \Omega} G_{\mathbf{Y}_r(P_{m-1})}(\omega)$
 and its corresponding \mathbf{x} vector estimate
 $\hat{\mathbf{x}}^T \leftarrow (\mathbf{a}_{\Phi}^H(\hat{\omega}) \mathbf{Y}_r(P_{m-1})) / \|\mathbf{a}_{\Phi}(\hat{\omega})\|_2^2$.
 - 6: $P'_m \leftarrow P_{m-1} \cup \{\hat{\mathbf{x}}, \hat{\omega}\}$
 - 7: **SINGLE REFINEMENT**: Refine $(\hat{\mathbf{x}}, \hat{\omega})$ using single frequency Newton update algorithm (R_s Newton steps) to obtain improved estimates $(\hat{\mathbf{x}}', \hat{\omega}')$.
 - 8: $P''_m \leftarrow P_{m-1} \cup \{\hat{\mathbf{x}}', \hat{\omega}'\}$
 - 9: **CYCLIC REFINEMENT**: Refine parameters in P''_m one at a time: For each $(\mathbf{x}, \omega) \in P''_m$, we treat $\mathbf{Y}_r(P''_m \setminus \{(\mathbf{x}, \omega)\})$ as the measurement \mathbf{Y} , and apply single frequency Newton update algorithm. We perform R_c rounds of cyclic refinements. Let P'''_m denote the new set of parameters.
 - 10: **UPDATE** all \mathbf{x} vector estimate in P'''_m by least squares: $\mathbf{A} \triangleq [\mathbf{a}_{\Phi}(\omega_1), \dots, \mathbf{a}_{\Phi}(\omega_m)], \{\omega_l\}$ are the frequencies in P'''_m . And $[\mathbf{x}_1, \dots, \mathbf{x}_m]^T = \mathbf{A}^\dagger \mathbf{Y}$.
 Let P_m denote the new set of parameters.
 - 11: **end while**
 - 12: **return** P_m
-

IV. STOPPING CRITERION

To understand the performance of Algorithm 1, the probability of the algorithm overestimating the model order K is of interest. An extreme scenario is that the proposed algorithm has detected K sinusoids which causes the residual to be only AWGN in the model (1), and the stopping criterion still isn't met. So the algorithm has to detect another sinusoid to make the residual decrease, which corresponds to the scenario of overestimating the model order.

We use the stopping criterion to estimate the model order K . If the residual energy can be well explained by noise, up to a target overestimating probability, then we stop. Intuitively, we choose to terminate the algorithm by comparing the magnitude of the Fourier transform of the residual with the expected noise power. Details are given in the next section.

A. Stopping criterion

The algorithm stops when

$$G_{\mathbf{Y}_r(P)}(\omega) = \sum_{i=1}^T |\langle \mathbf{y}_{ri}(P), \mathbf{a}(\omega) \rangle|^2 < \tau \quad (12)$$

for all DFT sampling frequencies $\{\omega_n \triangleq 2\pi n/N : n = 0, \dots, N-1\}$, where $\mathbf{y}_{ri}(P)$ is the i th column of $\mathbf{Y}_r(P)$, T is the number of snapshots and τ is the stopping threshold. Thus, we stop when $\sum_{i=1}^T \|\mathcal{F}\{\mathbf{y}_{ri}(P)\}\|_\infty^2 < \tau$, where $\mathcal{F}\{\mathbf{y}_{ri}(P)\}$ denotes the discrete Fourier transform of $\mathbf{y}_{ri}(P)$.

Supposedly, we have already correctly detected all sinusoids in the mixture. Under this condition, the residual is $\mathbf{y}_{ri}(P) \approx \mathbf{z}_i$, where $\mathbf{z}_i \sim \mathcal{CN}(\mathbf{0}, \sigma^2 \mathbf{I}_M)$. Note that $\mathcal{F}\{\cdot\}$ corresponds to a projection operation, so the statistics of AWGN are unchanged by it. Then by defining $R_n \triangleq \sum_{i=1}^T \|\mathbf{a}^H(\omega_n) \mathbf{z}_i\|_2^2$, we obtain

$$\Pr \left\{ \sum_{i=1}^T \|\mathcal{F}\{\mathbf{y}_{ri}(P)\}\|_\infty^2 > \tau \right\} = \Pr \left(\max_{n=1, \dots, N} R_n > \tau \right) = 1 - \Pr \left(\max_{n=1, \dots, N} R_n \leq \tau \right) = 1 - \Pr(R_1 \leq \tau, \dots, R_N \leq \tau) \quad (13)$$

Note that by defining $u_{n,i} = \mathbf{a}^H(\omega_n) \mathbf{z}_i$, we have

$$\mathbb{E} (u_{n_1, i_1} u_{n_2, i_2}^*) = \mathbb{E} [\mathbf{a}^H(\omega_{n_1}) \mathbf{z}_{i_1} \mathbf{z}_{i_2}^H \mathbf{a}(\omega_{n_2})] = \sigma^2 \delta_{i_1, i_2} \mathbb{E} [\mathbf{a}^H(\omega_{n_1}) \mathbf{a}(\omega_{n_2})] = \sigma^2 \delta_{i_1, i_2} \delta_{n_1, n_2}, \quad (14)$$

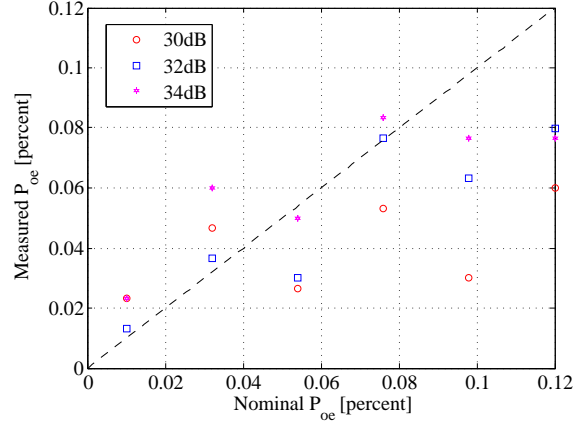


Fig. 1. Nominal vs measured probability of overestimating probability.

where δ_{i_1, i_2} denotes the dirichlet function, which equals zero unless $i_1 = i_2$ holds. From (14), we can conclude that R_n is a χ^2 random variable with $2T$ degrees of freedom. With the degrees of freedom being even, the cumulative distribution function (CDF) has a closed form given by

$$F_{2T}(R_n, \sigma^2) = \begin{cases} 1 - e^{-\frac{R_n}{\sigma^2}} \sum_{k=0}^{T-1} \frac{1}{k!} \left(\frac{R_n}{\sigma^2}\right)^k, & R_n > 0 \\ 0, & \text{otherwise.} \end{cases} \quad (15)$$

Therefore, (13) can be calculated as

$$\Pr \left\{ \sum_{i=1}^T \|\mathcal{F}\{\mathbf{y}_{ri}(P)\}\|_{\infty}^2 > \tau \right\} = 1 - [\Pr(R_n \leq \tau)]^N = 1 - F_{2T}(\tau, \sigma^2) = 1 - F_{2T}(\tau/\sigma^2, 1), \quad (16)$$

where $F_{2T}(R_n, 1)$ denotes the CDF of χ^2 random variable with unit variance.

Let P_{oe} denote a nominal overestimating probability. Thus P_{oe} satisfies

$$\Pr \left\{ \sum_{i=1}^T \|\mathcal{F}\{\mathbf{y}_{ri}(P)\}\|_{\infty}^2 > \tau \right\} = P_{oe}. \quad (17)$$

By defining $F_{2T}^{-1}(\cdot)$ as the inverse function of $F_{2T}(\cdot, 1)$, we obtain

$$\tau = \sigma^2 \left[F_{2T}^{-1} \left((1 - P_{oe})^{\frac{1}{N}} \right) \right] / 2. \quad (18)$$

Note that for a single snapshot, i.e., $T = 1$, $F_{2T}(R_n, \sigma^2) = 1 - e^{-R_n/\sigma^2}$ and $\tau = -\sigma^2 \log(1 - (1 - P_{oe})^{1/N})$ from (18), which is consistent with the results obtained in [18].

We conduct a numerical experiment by comparing the “measured” against “nominal” overestimating probability (17) to substantiate the above analysis. We use Algorithm 1 to estimate frequencies in a mixture of $K = 16$ sinusoids of the same fixed nominal SNR, defined as

$$\text{SNR}_l = 10 \times \log_{10} \left(\frac{\|\mathbf{a}(\omega_l) \mathbf{x}_l^T\|_{\mathbb{F}}^2}{\sigma^2 T} \right), \quad l = 1, \dots, K. \quad (19)$$

Furthermore, we generate the frequencies such that the minimal wrap-around frequency separation is $\Delta\omega_{\min}$, where $\Delta\omega_{\min} = \Delta\omega_{\text{DFT}}$ and the $\Delta\omega_{\text{DFT}} \triangleq 2\pi/N$ is the DFT grid separation. The parameters are set as follows: $N = 64$, $T = 10$, $R_s = 1$, $R_c = 3$, the number of Monte Carlo (MC) trials is 300. The “measured” overestimating probability is defined as the ratio of the overestimating events in all MC trials. From Fig. 1, it can be seen that the empirical overestimating probability is close to the nominal value at various SNRs, which means that the final residual error can be approximated as the AWGN, namely, the frequency estimation accuracy of Algorithm 1 is good.

B. Probability of Miss

Firstly, we define the neighborhood N_{ω_i} around the true frequency ω_i as $N_{\omega_i} \triangleq \{\omega : \text{dist}(\omega, \omega_i) \leq 0.25 \times \Delta_{\text{DFT}}\}$. Then we declare a miss of ω_i if none of the estimated frequencies locates in N_{ω_i} , otherwise we declare a successful detection of ω_i . Note that a miss is caused by both noise and inter-sinusoid interference, but we only discuss noise here.

Assuming no inter-sinusoid interference, the measurement \mathbf{Y} can be described as $\mathbf{Y} = [\mathbf{a}(\omega)x_1 + \mathbf{z}_1; \mathbf{a}(\omega)x_2 + \mathbf{z}_2; \dots; \mathbf{a}(\omega)x_T + \mathbf{z}_T]$. The signal frequency ω is not detected if

$$P_{\text{miss}} = \Pr \left\{ \|\mathbf{a}^H(\omega_d)\mathbf{Y}\|_2^2 < \tau \right\}, \quad (20)$$

where ω_d denotes the sampling frequency. Note that x_i is deterministic known, and $\mathbf{z}_i \sim \mathcal{CN}(0, \sigma^2 \mathbf{I}_N)$. Hence, we have

$$P_{\text{miss}} = \Pr \left\{ \sum_{i=1}^T |\mathbf{a}^H(\omega_d) [\mathbf{a}(\omega)x_i + \mathbf{z}_i]|^2 < \tau \right\}. \quad (21)$$

To calculate the above probability, we introduce

$$v_i \triangleq \mathbf{a}^H(\omega_d) [\mathbf{a}(\omega)x_i + \mathbf{z}_i] = x_i e^{j\frac{(N-1)(\omega-\omega_d)}{2}} \frac{\sin\left(\frac{N(\omega-\omega_d)}{2}\right)}{N \sin\left(\frac{\omega-\omega_d}{2}\right)} + \mathbf{a}^H(\omega_d)\mathbf{z}_i. \quad (22)$$

By defining

$$\alpha \triangleq \frac{\sin[N(\omega - \omega_d)/2]}{N \sin[(\omega - \omega_d)]/2}, \quad (23a)$$

$$\tilde{R}_m \triangleq \|\mathbf{a}^H(\omega_d)\mathbf{Y}\|_2^2 = \sum_{i=1}^T |v_i|^2, \quad (23b)$$

we can conclude that \tilde{R}_m is a noncentral χ^2 random variable with $2T$ degrees of freedom and common variance being $\sigma^2/2$. With degrees of freedom being an even number, the CDF of \tilde{R}_m can be written in the form

$$F_{2T}(\tilde{R}_m) = \begin{cases} 1 - Q_T\left(\frac{\sqrt{2}s}{\sigma}, \frac{\sqrt{2\tilde{R}_m}}{\sigma}\right), & \tilde{R}_m > 0 \\ 0, & \end{cases} \quad (24)$$

where Q_T denotes Marcum Q-function and s is defined as

$$s \triangleq \alpha \sqrt{\sum_{i=1}^T |x_i|^2}. \quad (25)$$

Thus it's easy to show that

$$P_{\text{miss}} = 1 - Q_T\left(\alpha \sqrt{2 \sum_{i=1}^T |x_i|^2 / \sigma}, \sqrt{2\tau / \sigma^2}\right). \quad (26)$$

Supposing a frequency within a DFT grid interval follows the uniform distribution, then we obtain $E[\alpha] = 0.88$, where $\omega \sim \mathcal{U}[-\pi/N, \pi/N]$. Hence,

$$P_{\text{miss}} = 1 - Q_T\left(0.88 \sqrt{2 \sum_{i=1}^T |x_i|^2 / \sigma}, \sqrt{2\tau / \sigma^2}\right). \quad (27)$$

V. CONVERGENCE

In this section, the convergence of the proposed algorithm is studied. Firstly, upper bounds on the number of iterations needed to reach the stopping condition are given. Then a bound on the rate of convergence of Algorithm 1 is provided, which is a function of the ‘‘atomic norm’’ of original measurements \mathbf{Y} and the oversampling factor γ . Here, we only consider the uncompressed scenario, namely, $\Phi = \mathbf{I}_N$.

A. Proof of convergence

It's easy to show that the number of measurements N is a trivial upper bound of the number of iterations of Algorithm 1. From step 10 of Algorithm 1, it can be shown that \mathbf{X} becomes a square full-rank matrix (note that there is no frequency that will be detected twice) after N iterations. Then the algorithm terminates because the residual is equal to zero for $(N + 1)$ th iteration.

In the following, we provide another upper bound on the number of iterations, which is obtained by considering how much the residual energy will decrease when a new frequency is added to the set of estimated sinusoids.

Theorem 1 Let $\|\mathbf{Y}\|_{\mathbb{F}}^2$ be the original residual energy. When a new frequency is added to the set of estimated sinusoids, the reduction of residual energy is at least τ . Consequently, $\min\{N, \lfloor \|\mathbf{Y}\|_{\mathbb{F}}^2/\tau \rfloor\}$ is an upper bound on the number of iterations of the Algorithm 1.

PROOF Assume we have detected m sinusoids, the residual measurement is given by $\mathbf{Y}_r(P_m) = \mathbf{Y} - \sum_{l=1}^m \mathbf{a}(\omega_l) \mathbf{x}_l^H$. The residual energy in each iteration step of the Algorithm 1 satisfies the following,

$$\begin{aligned} \|\mathbf{Y}_r(P_{m-1})\|_{\mathbb{F}}^2 &\stackrel{(a)}{=} \|\mathbf{Y}_r(P'_m)\|_{\mathbb{F}}^2 + G_{\mathbf{Y}_r(P_{m-1})}(\hat{\omega}) \stackrel{(b)}{\geq} \|\mathbf{Y}_r(P''_m)\|_{\mathbb{F}}^2 + G_{\mathbf{Y}_r(P_{m-1})}(\hat{\omega}) \stackrel{(c)}{\geq} \|\mathbf{Y}_r(P_m)\|_{\mathbb{F}}^2 + G_{\mathbf{Y}_r(P_{m-1})}(\hat{\omega}) \quad (28) \\ &\stackrel{(d)}{\geq} \|\mathbf{Y}_r(P_m)\|_{\mathbb{F}}^2 + \tau. \quad (29) \end{aligned}$$

where $\hat{\omega}$ denotes the detected frequency. Equality in (a) holds because of the step 5 in the Algorithm 1 where we project $\mathbf{Y}_r(P_{m-1})$ orthogonal to the subspace spanned by $\mathbf{a}(\hat{\omega})$ to get $\mathbf{Y}_r(P'_m)$. Basically, we get $[\mathbf{Y}_r(P_{m-1}) - \mathbf{a}(\hat{\omega}) \mathbf{x}_m^H]^H \mathbf{a}(\hat{\omega}) = \mathbf{0}$ and $\mathbf{x}_m^H = [\mathbf{a}(\hat{\omega})^H \mathbf{Y}_r(P_{m-1})] / \|\mathbf{a}(\hat{\omega})\|_2^2$ by solving $\min_{\mathbf{x}_m} \|\mathbf{Y}_r(P_{m-1}) - \mathbf{a}(\hat{\omega}) \mathbf{x}_m^H\|_{\mathbb{F}}^2$. Then we take the Frobenius norm of both sides of $\mathbf{Y}_r(P'_m) = \mathbf{Y}_r(P_{m-1}) - \mathbf{a}(\hat{\omega}) \mathbf{x}_m^H$ to obtain equality (a). Inequality in (b) follows from RAC, which is implemented whenever the single refinement step is executed and (c) is a direct consequence of the step 10 of the Algorithm 1, which can only cause a decrease in the residual energy. And the stopping criterion leads to (d).

From inequality (29), we can conclude that the reduction of the residual energy caused by the detection of a new sinusoid frequency is always larger than τ . Thus we can get another bound on the number of iterations of Algorithm 1, which is $\lfloor \|\mathbf{Y}\|_{\mathbb{F}}^2/\tau \rfloor$. ■

B. Rate of convergence

In the uncompressed and noiseless scenario, the noiseless measurement \mathbf{Y}^o can be written as

$$\mathbf{Y}^o = \sum_{k=1}^K \mathbf{a}(\omega_k) \mathbf{x}_k^H = \sum_{k=1}^K c_k \mathbf{a}(\omega_k) \phi_k^H. \quad (30)$$

where $c_k = \|\mathbf{x}_k\|_2 > 0$, $\omega_k \in [0, 2\pi)$, $\phi_k = c_k^{-1} \mathbf{x}_k \in \mathbb{C}^{T \times 1}$ with $\|\phi_k\|_2 = 1$. Then the continuous dictionary or the set of atoms is given as

$$\mathcal{A} \triangleq \{\mathbf{A}(\omega, \phi) = \mathbf{a}(\omega) \phi^H : \omega \in [0, 2\pi), \|\phi\|_2 = 1\}. \quad (31)$$

It is easy to see that \mathbf{Y}^o is a linear combination of many atoms in \mathcal{A} . Here, we define the atomic ℓ_0 (pseudo-) norm of $\mathbf{Y} \in \mathbb{C}^{N \times T}$ as the smallest number of atoms that can express it:

$$\|\mathbf{Y}\|_{\mathcal{A},0} = \inf_{\mathcal{K}} \left\{ \mathbf{Y} = \sum_{k=1}^{\mathcal{K}} c_k \mathbf{A}(\omega_k, \phi_k), c_k \geq 0 \right\}. \quad (32)$$

Because the atomic ℓ_0 norm is non-convex, we utilize convex relaxation to relax the atomic ℓ_0 norm to the atomic norm, which is defined as the gauge function of $\text{conv}(\mathcal{A})$, where $\text{conv}(\mathcal{A})$ is the convex hull of \mathcal{A} :

$$\|\mathbf{Y}\|_{\mathcal{A}} \triangleq \inf\{t > 0 : \mathbf{Y} \in t \text{conv}(\mathcal{A})\} = \inf \left\{ \sum_k c_k : \mathbf{Y} = \sum_k c_k \mathbf{A}(\omega_k, \phi_k), c_k \geq 0 \right\}. \quad (33)$$

By defining $\langle \mathbf{Y}, \mathbf{A} \rangle = \text{tr}(\mathbf{A}^H \mathbf{Y})$ and $\langle \mathbf{Y}, \mathbf{A} \rangle_{\mathbb{R}} = \Re(\langle \mathbf{Y}, \mathbf{A} \rangle)$, the dual norm of $\|\mathbf{Y}\|_{\mathcal{A}}$ can be written as

$$\begin{aligned} \|\mathbf{Y}\|_{\mathcal{A}}^* &\triangleq \sup_{\|\mathbf{A}\|_{\mathcal{A}} \leq 1} \langle \mathbf{Y}, \mathbf{A} \rangle_{\mathbb{R}} \\ &= \sup_{\omega \in [0, 2\pi), \|\phi\|_2 = 1} \langle \mathbf{Y}, \mathbf{a}(\omega) \phi^H \rangle_{\mathbb{R}} = \sup_{\omega \in [0, 2\pi), \|\phi\|_2 = 1} |\langle \phi, \mathbf{Y}^H \mathbf{a}(\omega) \rangle| = \sup_{\omega \in [0, 2\pi)} \|\mathbf{Y}^H \mathbf{a}(\omega)\|_2 = \sup_{\omega \in [0, 2\pi)} \sqrt{G_{\mathbf{Y}}(\omega)}, \quad (34) \end{aligned}$$

where the $G_{\mathbf{Y}}(\omega)$ is (7).

Theorem 2 Maximizing $G_{\mathbf{Y}}(\omega)$ (for the dictionary of unit norm sinusoids) over $[0, 2\pi)$ is consistent with that over the oversampled grid Ω with oversampling factor γ . Namely, we have

$$\max_{\omega \in \Omega} \sqrt{G_{\mathbf{Y}}(\omega)} \leq \sup_{\omega \in [0, 2\pi)} \sqrt{G_{\mathbf{Y}}(\omega)} \leq \left(1 - \frac{4\pi T}{\gamma}\right)^{-1/2} \max_{\omega \in \Omega} \sqrt{G_{\mathbf{Y}}(\omega)} \quad (35)$$

PROOF According to (34), $(\|\mathbf{Y}\|_{\mathcal{A}}^*)^2$ can be expressed as

$$(\|\mathbf{Y}\|_{\mathcal{A}}^*)^2 = \sup_{\omega \in [0, 2\pi)} \|\mathbf{Y}^H \mathbf{a}(\omega)\|_2^2 = \sup_{\omega \in [0, 2\pi)} \sum_{t=1}^T \left| \frac{1}{\sqrt{N}} \sum_{n=1}^N \phi_{n,t}^* e^{j(n-1)\omega} \right|^2 = \sup_{\omega \in [0, 2\pi)} \sum_{t=1}^T |W_t(\omega)|^2, \quad (36)$$

where $\phi_{n,t}$ is the (n,t) th entry of \mathbf{Y} , and $W_t(\omega) \triangleq \frac{1}{\sqrt{N}} \sum_{n=1}^N \phi_{n,t}^* e^{j(n-1)\omega}$. For $\omega_1, \omega_2 \in [0, 2\pi)$, according to Bernstein's theorem [20] and the result in [21] (Appendix C), we can obtain

$$|W_t(\omega_1)| - |W_t(\omega_2)| \leq 2N|\omega_1 - \omega_2| \sup_{\omega \in [0, 2\pi)} |W_t(\omega)|. \quad (37)$$

Then we have

$$\begin{aligned} \sum_{t=1}^T |W_t(\omega_1)|^2 - \sum_{t=1}^T |W_t(\omega_2)|^2 &\stackrel{(a)}{\leq} \sum_{t=1}^T (|W_t(\omega_1)| + |W_t(\omega_2)|) \left(2N|\omega_1 - \omega_2| \sup_{\omega \in [0, 2\pi)} |W_t(\omega)| \right) \\ &\stackrel{(b)}{\leq} 4N|\omega_1 - \omega_2| T \sup_{\omega \in [0, 2\pi)} \sum_{t=1}^T |W_t(\omega)|^2 = 4N|\omega_1 - \omega_2| T (\|\mathbf{Y}\|_{\mathcal{A}}^*)^2, \end{aligned} \quad (38)$$

where inequality (a) follows from plugging in (37), inequality (b) is from the fact that

$$\sum_{t=1}^T \sup_{\omega \in [0, 2\pi)} |W_t(\omega)|^2 \leq T \sup_{\omega \in [0, 2\pi)} \sum_{t=1}^T |W_t(\omega)|^2, \text{ and the last equality follows by (36).}$$

Let ω_2 take any value of the grid points $\left\{0, \frac{2\pi}{\gamma N}, \dots, \frac{2\pi(\gamma N - 1)}{\gamma N}\right\}$, we have

$$\begin{aligned} (\|\mathbf{Y}\|_{\mathcal{A}}^*)^2 &= \sup_{\omega \in [0, 2\pi)} \sum_{t=1}^T |W_t(\omega)|^2 = \sup_{\omega \in [0, 2\pi)} \sum_{t=1}^T \left(|W_t(\omega)|^2 - |W_t(\tilde{\omega})|^2 + |W_t(\tilde{\omega})|^2 \right) \\ &\leq \sup_{\omega \in [0, 2\pi)} \sum_{t=1}^T \left(|W_t(\omega)|^2 - |W_t(\tilde{\omega})|^2 \right) + \max_{d=0, \dots, \gamma N - 1} \sum_{t=1}^T \left| W_t \left(\frac{2\pi d}{\gamma N} \right) \right|^2 \\ &\leq 4N|\omega - \tilde{\omega}| T (\|\mathbf{Y}\|_{\mathcal{A}}^*)^2 + \max_{d=0, \dots, \gamma N - 1} \sum_{t=1}^T \left| W_t \left(\frac{2\pi d}{\gamma N} \right) \right|^2 \\ &\leq 4N \frac{2\pi}{2\gamma N} T (\|\mathbf{Y}\|_{\mathcal{A}}^*)^2 + \max_{d=0, \dots, \gamma N - 1} \sum_{t=1}^T \left| W_t \left(\frac{2\pi d}{\gamma N} \right) \right|^2 \\ &= \frac{4\pi T}{\gamma} (\|\mathbf{Y}\|_{\mathcal{A}}^*)^2 + \max_{d=0, \dots, \gamma N - 1} \sum_{t=1}^T \left| W_t \left(\frac{2\pi d}{\gamma N} \right) \right|^2 \end{aligned} \quad (39)$$

Since the maximum on the grid is a lower bound for $(\|\mathbf{Y}\|_{\mathcal{A}}^*)^2$, we have

$$\left(\max_{d=0, \dots, \gamma N - 1} \sum_{t=1}^T \left| W_t \left(\frac{2\pi d}{\gamma N} \right) \right|^2 \right)^{1/2} \leq \|\mathbf{Y}\|_{\mathcal{A}}^* \leq \left(1 - \frac{4\pi T}{\gamma} \right)^{-1/2} \left(\max_{d=0, \dots, \gamma N - 1} \sum_{t=1}^T \left| W_t \left(\frac{2\pi d}{\gamma N} \right) \right|^2 \right)^{1/2} \quad (40)$$

Thus,

$$\max_{\omega \in \Omega} \sqrt{G_{\mathbf{Y}}(\omega)} \leq \sup_{\omega \in [0, 2\pi)} \sqrt{G_{\mathbf{Y}}(\omega)} \leq \left(1 - \frac{4\pi T}{\gamma} \right)^{-1/2} \max_{\omega \in \Omega} \sqrt{G_{\mathbf{Y}}(\omega)}. \quad (41)$$

■

To prove Theorem 3, the following lemma in [22] is introduced

Lemma 1 [22] Assume $\{a_n\}_{n \geq 0}$ is a decreasing sequence of nonnegative numbers such that $a_0 \leq U$ and

$$a_n \leq a_{n-1} \left(1 - \frac{a_{n-1}}{U} \right), \forall n > 0, \quad (42)$$

then we have $a_n \leq \frac{U}{n+1}$ for all $n \geq 0$.

Theorem 3 For all \mathbf{Y} satisfying $\|\mathbf{Y}\|_{\mathcal{A}} < \infty$, the residual energy of Algorithm 1 at the m th iteration satisfies

$$\|\mathbf{Y}_r(P_m)\|_{\mathbb{F}} \leq (m+1)^{-1/2} \left(1 - \frac{4\pi T}{\gamma} \right)^{-1/2} \|\mathbf{Y}\|_{\mathcal{A}}. \quad (43)$$

PROOF From (28), we have

$$\|\mathbf{Y}_r(P_m)\|_{\mathbb{F}}^2 \leq \|\mathbf{Y}_r(P_{m-1})\|_{\mathbb{F}}^2 - G_{\mathbf{Y}_r(P_{m-1})}(\hat{\omega}). \quad (44)$$

$\mathbf{Y}_r(P_{m-1})$ is a direct consequence of projecting \mathbf{Y} orthogonal to the subspace spanned by P_{m-1} , therefore

$$\begin{aligned} \|\mathbf{Y}_r(P_{m-1})\|_{\mathbb{F}}^2 &= \langle \mathbf{Y}_r(P_{m-1}), \mathbf{Y} \rangle_{\mathbb{R}} \stackrel{(a)}{\leq} \|\mathbf{Y}\|_{\mathcal{A}} \|\mathbf{Y}_r(P_{m-1})\|_{\mathcal{A}}^* = \|\mathbf{Y}\|_{\mathcal{A}} \sup_{\omega \in [0, 2\pi)} \sqrt{G_{\mathbf{Y}_r(P_{m-1})}(\omega)} \\ &\stackrel{(b)}{\leq} \|\mathbf{Y}\|_{\mathcal{A}} \left(1 - \frac{4\pi T}{\gamma}\right)^{-1/2} \max_{\omega \in \Omega} \sqrt{G_{\mathbf{Y}_r(P_{m-1})}(\omega)}, \end{aligned} \quad (45)$$

where inequality (a) follows from the following

$$\|\mathbf{Y}_r(P_{m-1})\|_{\mathcal{A}}^* = \sup_{\|\mathbf{Y}\|_{\mathcal{A}} \leq 1} \langle \mathbf{Y}, \mathbf{Y}_r(P_{m-1}) \rangle_{\mathbb{R}} \geq \left\langle \frac{\mathbf{Y}}{\|\mathbf{Y}\|_{\mathcal{A}}}, \mathbf{Y}_r(P_{m-1}) \right\rangle_{\mathbb{R}} \quad (46)$$

and equality (b) is obtained from Theorem 2. From the step 5 of the Algorithm 1, we have

$$\hat{\omega} = \arg \max_{\omega \in \Omega} \sqrt{G_{\mathbf{Y}_r(P_{m-1})}(\omega)}, \quad (47)$$

By defining $\eta \triangleq \|\mathbf{Y}\|_{\mathcal{A}} \left(1 - \frac{4\pi T}{\gamma}\right)^{-1/2}$ and combing with (47), we have

$$\|\mathbf{Y}_r(P_{m-1})\|_{\mathbb{F}}^2 \leq \eta \sqrt{G_{\mathbf{Y}_r(P_{m-1})}(\hat{\omega})}. \quad (48)$$

Combining (44) and (48), yields

$$\|\mathbf{Y}_r(P_m)\|_{\mathbb{F}}^2 \leq \|\mathbf{Y}_r(P_{m-1})\|_{\mathbb{F}}^2 (1 - \eta^{-2} \|\mathbf{Y}_r(P_{m-1})\|_{\mathbb{F}}^2). \quad (49)$$

By using Lemma 1 and the fact that

$$\|\mathbf{Y}_r(P_0)\|_{\mathbb{F}}^2 = \|\mathbf{Y}\|_{\mathbb{F}}^2 \stackrel{(a)}{\leq} \|\mathbf{Y}\|_{\mathcal{A}}^2 \leq \eta^2, \quad (50)$$

where inequality (a) follows from (51)

$$\begin{aligned} \|\mathbf{Y}\|_{\mathbb{F}}^2 &= \text{tr}\{\mathbf{Y}^H \mathbf{Y}\} = \text{tr} \left\{ \sum_{k=1}^K \sum_{l=1}^K \mathbf{x}_k \mathbf{a}^H(\omega_k) \mathbf{a}(\omega_l) \mathbf{x}_l^H \right\} = \text{tr} \left\{ \sum_{k=1}^K \sum_{l=1}^K |\mathbf{x}_l^H \mathbf{x}_k| |\mathbf{a}^H(\omega_k) \mathbf{a}(\omega_l)| \right\} \leq \sum_{k=1}^K \sum_{l=1}^K |\mathbf{x}_l^H \mathbf{x}_k| \\ &\leq \sum_{k=1}^K \sum_{l=1}^K \|\mathbf{x}_k\|_2 \|\mathbf{x}_l\|_2 = \|\mathbf{Y}\|_{\mathcal{A}}^2 \end{aligned} \quad (51)$$

we have

$$\|\mathbf{Y}_r(P_m)\|_{\mathbb{F}}^2 \leq \frac{\eta^2}{m+1}. \quad (52)$$

In other words,

$$\|\mathbf{Y}_r(P_m)\|_{\mathbb{F}} \leq (m+1)^{-1/2} \left(1 - \frac{4\pi T}{\gamma}\right)^{-1/2} \|\mathbf{Y}\|_{\mathcal{A}}. \quad (53)$$

This proves the Theorem 3. ■

Note that the component in (53) is $(1 - 4\pi T/\gamma)^{-1/2}$ instead of $(1 - 2\pi/\gamma)^{-1}$ in [18]. Given $T = 1$, our conclusion isn't consistent with that in [18]. In fact, due to $(1 - 4\pi T/\gamma)^{-1/2} \geq (1 - 2\pi/\gamma)^{-1}$, the bound on the rate of convergence is tighter in the single snapshot scenario.

C. Empirical rate of convergence

The relative residual energy of the i th iteration (averaged over 300 runs) versus the number of iterations in a noiseless scenario is plotted to show the effects of the refinement steps on the convergence of Algorithm 1, defined as $20 \log_{10} (\|\mathbf{Y}_r(P_m)\|_{\mathbb{F}} / \|\mathbf{Y}\|_{\mathcal{A}})$. Here, we compare Algorithm 1 in the scenarios of $T = 1$ and $T = 10$ to the following variants of OMP to show the improvements brought by the refinement steps.

NOMP without cyclic refinements in MMV setting: This is an algorithm that has a nearly comparable performance with OMP [23] over the continuum of atoms. We use Algorithm 1 to implement this method by setting the number of cyclic refinement steps to 0. This algorithm lies in the class of forward greedy methods because it doesn't have a feedback mechanism. Hence, our analysis is also applicable to this method.

Discretized OMP: If we skip the single and cyclic refinement steps, then we can obtain a standard OMP applied to the oversampled grid Ω . Note that this algorithm can be viewed as a special case of Algorithm 1, so the convergence analysis

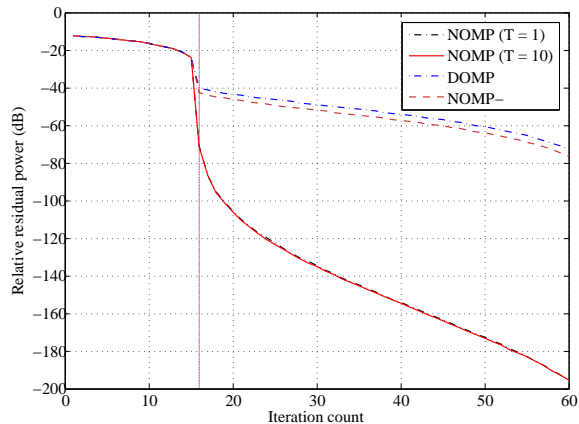


Fig. 2. Convergence rates at noiseless case.

results are also valid. The parameters are set as follows: $K = 16$, $N = 64$, $T = 10$, $R_s = 1$, $R_c = 1$, $\text{SNR} = 25$ dB, $\Delta\omega_{\min} = 2.5\Delta\omega_{\text{DFT}}$. From Fig. 2, it can be shown that a small oversampling factor ($\gamma = 4$) with single refinement step (NOMP-) has a slightly faster convergence than a large oversampling factor ($\gamma = 20$) with no refinements (DOMP). Furthermore, we can see a large gap between Algorithm 1 and the other two algorithms, which means that the cyclic refinement steps lead to an extremely fast convergence for Algorithm 1. In Fig. 2, we can see that the residual energy drops sharply at the 16th iteration, which is equal to the number of sinusoids in the mixture K . Furthermore, it can be seen that increasing the number of snapshots has a slight effect on the convergence rate.

VI. SIMULATION

In this section, we conduct numerical simulations to compare the performance of the proposed Algorithm 1 against other methods in terms of estimation accuracy in various scenarios.

Benchmarks: All algorithms are compared against the DFT method implemented by coarsely picking out the top K peaks, and the oversampling rate for DFT is set to 4.

For the classical subspace method, we choose the MUSIC method to estimate frequencies of sinusoids in the mixture. Specifically, we make one modification based on the version of the MATLAB rootmusic algorithm. In detail, a sliding window of size W is adopted to obtain an estimate of the covariance matrix of the measurement data. Different choices of W have a considerable impact on the estimation accuracy. In particular, if W is set too large, the estimation performance of the signal subspace and the autocorrelation matrix will degrade. Whereas a small W will result in a less accurate frequency estimation performance. Empirically, we found that $W = 44$ results in the best estimation performance in our all four scenarios. It's worth mentioning that, instead of implementing an empirical method to estimate K , we just directly feed the true K to the solver.

Newtonized BPDN: For the sparse method inspired by sparse representation, we employ the SPGL1 toolbox [24] to solve the $l_{2,1}$ minimization problem, also known as the MMV version of BPDN, we denote this method simply as BPDN in the following, which is defined as

$$\min \|\mathbf{X}\|_{1,2} \text{ subject to } \|\mathbf{A}\mathbf{X} - \mathbf{Y}\|_{\text{F}} \leq \tau, \quad (54)$$

where $\|\mathbf{X}\|_{1,2}$ denotes the sum of the two-norms of the rows of \mathbf{X} and τ is the measure of the noise level. Newtonized BPDN can be viewed as an extension of the BPDN method. By applying this toolbox to model (1) in the scenario of $\Phi = \mathbf{I}_N$, where the oversampling rate is set to 4 and $\tau = \sqrt{NT}\sigma^2$, we then obtain the optimized \mathbf{X} . By sorting the two-norms of every row of the estimated \mathbf{X} in a descending order, we choose the K frequencies that correspond to the top K two-norms of every row of the estimated \mathbf{X} as the estimated frequencies. To avoid the frequency splitting phenomenon [25, 26], we impose an extra procedure to the Newtonized BPDN method to cope with two special cases. On the one hand, when the interval between two adjacent estimated frequencies sorted in an ascending order is smaller or equal to $2\pi/(\gamma N)$, we eliminate the latter frequency. At the same time we add the frequency corresponding to the top $K + 1$ th two-norms of the row of the estimated \mathbf{X} . On the other hand, we also adopt the afore-mentioned step to improve the estimation performance when the first and last element of the sorted frequencies are equal to 0 and the last sampling frequency, respectively. We recycle the whole procedure until there is no occurrence of those two incidents. Then we apply the cyclic refinement step of the Algorithm 1 to the estimated frequencies, and we set $R_c = 1$, $R_s = 1$ in this case.

We adopt the SPA with a uniform linear array (ULA) method defined in [15] to implement sparse convex optimization. We made one modification to avoid the frequency splitting phenomenon. Specifically, according to the [15], when optimized \mathbf{u}^* is obtained by solving a semidefinite programming problem, we then perform eigenvalue decomposition on $T(\mathbf{u}^*)$ and treat

the smallest eigenvalue as the noise variance denoted by $\hat{\sigma}^2$. Here $T(\mathbf{u}^*)$ is a Toeplitz matrix constructed by \mathbf{u}^* . Finally, we treat $T(\mathbf{u}^*) - \text{diag}(\hat{\sigma}^2)$ and the true model order K as the input parameters of the MATLAB rootmusic algorithm.

For the IRA algorithm [17], we generalize the single snapshot method to the scenario with MMVs. Considering the huge computation cost, we set the oversampling rate to 2. Other system parameters are kept unchanged.

For the NOMP algorithm with MMVs, the corresponding partial parameters in various settings are summarized in Table II. We don't require explicit estimates of model order and set the overestimating probability to 0.01. All possible situations can be divided into three cases: 1) The estimated model order is smaller than K . 2) We successfully detected K frequencies. In this case, we directly calculate the NMSE. 3) The last case is that we overestimate the model order. If we encounter this situation, we firstly sort the $\text{diag}(\mathbf{X}^H \mathbf{X})$ and choose the K frequencies corresponding to the top K elements of the $\text{diag}(\mathbf{X}^H \mathbf{X})$ as the estimated frequencies. Then we take the same procedure to avoid frequency splitting as used in the Newtonized BPDN algorithm.

Simulation Set-up: Here, we concentrate on estimating a mixture of $K = 16$ complex sinusoids with length $N = 64$ in the uncompressed scenario. The number of snapshots is $T = 10$ and the noise variance is equal to 1. Each scenario, as defined by $\Delta\omega_{\min}$ and SNR (19) is implemented over 300 MC trials. The original frequencies of the sinusoids in the mixture are sampled from $[0, 2\pi)$ and meet the corresponding minimum separation criterion. The detailed settings are shown in Table I. In the following, we aim at obtaining the frequency estimation accuracy performance of the Algorithm 1 as compared to the other methods in terms of error distribution and mean squared error.

TABLE I
SETTINGS OF DIFFERENT SCENARIOS.

Scenarios	SNR (dB)	$\Delta\omega_{\min}/\Delta\omega_{\text{DFT}}$
1	SNR_{nom}	2.5
2	SNR_{nom}	1
3	Uniform[15, 35]	2.5
4	Uniform[15, 35]	1

TABLE II
PARAMETERS OF ALGORITHM 1 IN DIFFERENT SCENARIOS.

Algorithm 1	Scenario 1	Scenario 2	Scenario 3	Scenario 4
R_c	1	3	1	3
R_s	1	1	1	1

TABLE III
TIME [SEC] AVERAGED OVER 300 RUNS OF EACH ALGORITHM. PARAMETERS OF ALGORITHM 1 ARE SET BY II

Time [sec]	MUSIC	M-BPDN	NOMP	SPA	IRA
Scenario 1	0.011	0.069	0.163	37.919	184.516
Scenario 2	0.011	0.066	0.282	40.082	250.091
Scenario 3	0.012	0.060	0.168	36.455	278.857
Scenario 4	0.011	0.064	0.279	39.381	229.402

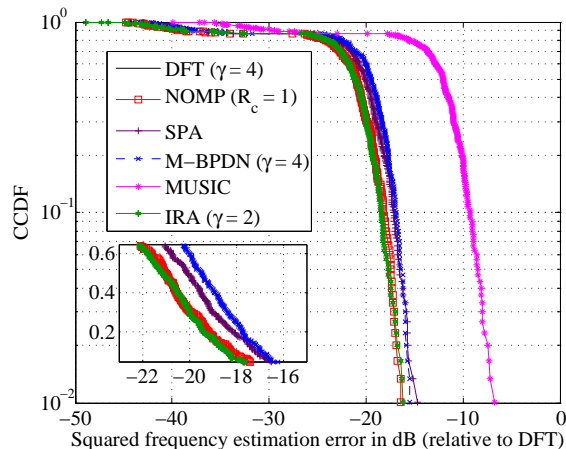
A. Error Distribution

Firstly, we plot the Complementary Cumulative Distribution Function (CCDF) of the squared frequency estimation error for all algorithms to study the error distribution. In scenario 1 and 2, SNR_{nom} is set as 25 dB for all sinusoids in the mixture. As for scenario 3 and 4, the SNR corresponding to each sinusoid is selected independently and uniformly from [15, 35] dB. It should be mentioned that all the algorithms are compared against the DFT method, which is implemented by coarse peak peaking.

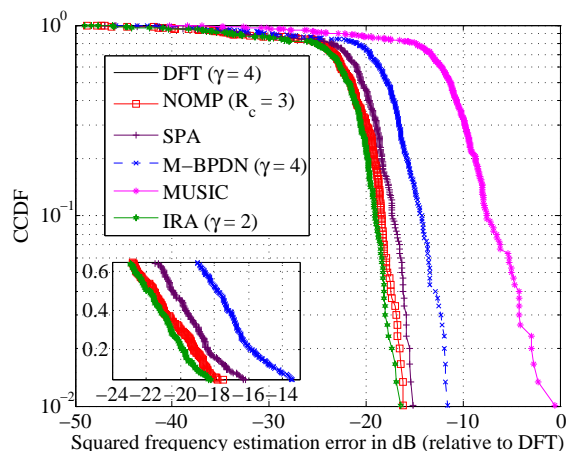
From Fig. 3, we can see that the IRA and the NOMP algorithm have a comparable performance, and both of them have the highest estimation accuracy compared to the SPA and the M-BPDN algorithm. All those four methods outperform the MUSIC algorithm in Scenario 1. The observation that the M-BPDN algorithm has a near-optimal performance shows that BPDN has a very good estimation of the true frequencies. While in Scenario 2, the performance of the M-BPDN algorithm degrades because the frequencies are becoming closer to each other. The MUSIC algorithm also suffers from the small separation between frequencies.

The error distribution in Scenarios 3 and 4 are demonstrated in Fig. 4. In this scenario, we can still see that IRA and NOMP algorithms have a very similar error distribution, but the gap between those two algorithms and other methods has increased. In those two scenarios, SPA outperforms M-BPDN considerably compared to Scenario 1. When frequencies are closer, it can

be seen that the span of squared frequency estimation error has enlarged. The performance of all algorithms degrades in the scenario where frequencies are harder to identify, but IRA and NOMP algorithms still achieve a much better performance. From Table III, we can conclude that the MUSIC algorithm is the fastest algorithm among all these algorithms. The NOMP algorithm has a better performance but a slower speed compared to the M-BPDN algorithm. The computation costs of SPA and IRA are large, where the latter method is the slowest but almost always achieves the best estimation accuracy.



(a) Scenario 1



(b) Scenario 2

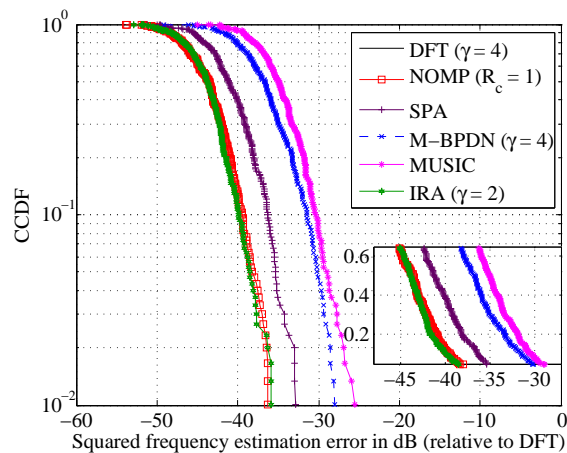
Fig. 3. CCDF of the frequency MSE for Scenario 1 and 2.

B. Mean squared error

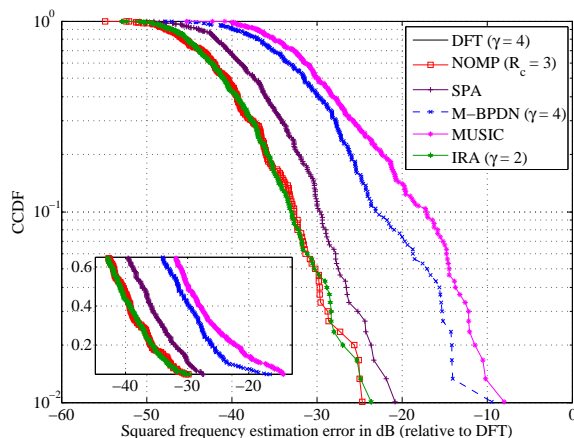
In this part, we aim to compare the estimation performance of all algorithms by using NMSE and CRB in all four scenarios. Our goal is to obtain the estimation performance of a single sinusoid (ignoring the other sinusoids). Considering the huge computation cost of IRA algorithm, we decide not to consider it in this section.

In scenario 1 and 2, SNR_{nom} takes values from 5 dB to 35 dB. We regard the mean value of CRB of all K sinusoids as the CRB corresponding to a single sinusoid. The NMSE is defined as $E[\|\omega_{\text{est}} - \omega_{\text{true}}\|_2^2] / \Delta_{\text{DFT}}^2$. For scenarios 3 and 4, we keep the SNR of one of the sinusoids at a given value taken from [5, 35] dB, while the other $(K - 1)$ SNRs are drawn independently and uniformly from [15, 35] dB. In these two scenarios, the NMSE is $|\omega_{\text{est}} - \omega_{\text{true}}|^2 / \Delta_{\text{DFT}}^2$, where ω_{true} denotes the sinusoid according to the fixed SNR. We choose the CRB that corresponds to this sinusoid to plot along with NMSE.

Fig. 5 shows the MSE of frequency estimation in Scenario 1 and 2. We can see that NOMP achieves the CRB when SNR is equal to 9 dB and it benefits from increasing the SNR in Scenario 1. SPA almost achieves the CRB at a smaller SNR value compared to the NOMP method and likewise achieves a better estimation performance as SNR increases. On the other hand, the M-BPDN algorithm achieves performance floors when SNR is bigger than 29 dB. Although the MUSIC algorithm follows the bound when SNR is bigger than 15 dB, it doesn't achieve the CRB. In scenario 2, we can see that the NOMP and SPA



(a) Scenario 3



(b) Scenario 4

Fig. 4. CCDF of the frequency MSE for Scenario 3 and 4.

algorithm almost equal to CRB as SNR increases. The NOMP algorithm slightly deviates from CRB when SNR is larger than 25 dB. The M-BPDN method reaches performance floors at a smaller SNR value compared to Scenario 1. MUSIC benefits from increasing the SNR and the gap between MUSIC and CRB is larger than Scenario 1.

Fig. 6 (a) corresponds to Scenario 3. It shows that NOMP achieves CRB earlier than any other method and doesn't reach performance floors. SPA benefits from increasing the SNR and becomes closer to CRB. The M-BPDN algorithm reaches performance floors at a large SNR values and has less accurate performance compared to MUSIC. The same observations can also be applicable to Scenario 4, where the separation between frequencies is small.

VII. CONCLUSION

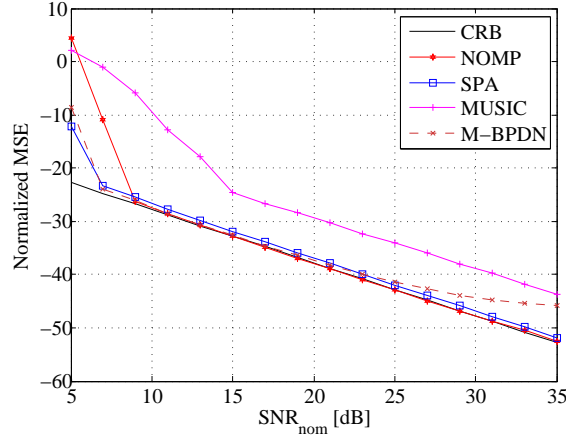
The NOMP algorithm is extended to deal with MMVs settings. The algorithm uses the information of already detected frequencies to refine the current frequency and has a stopping criterion based on a given overestimating probability. The convergence results are provided. Compared to the classical MUSIC algorithm, more recent SPA and M-BPDN algorithm, the NOMP algorithm has a superior performance in terms of frequency estimation accuracy and asymptotically approaches the CRB. As for the run time, the NOMP algorithm is much faster than the SPA and IRA method.

VIII. APPENDIX: ESTIMATION THEORETIC BOUNDS

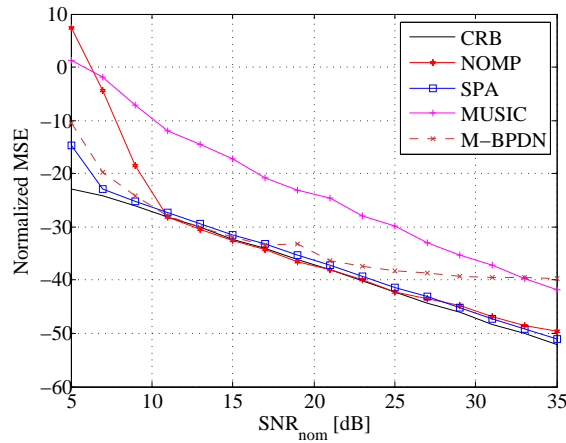
Given the observation vector \mathbf{y} which determines the estimator $\hat{\boldsymbol{\theta}}(\mathbf{y})$, a widely used criterion to characterize the performance of the estimator is the mean square error (MSE), given by

$$\text{mse}(\hat{\boldsymbol{\theta}}(\mathbf{y})) = \mathbb{E}_{\mathbf{y};\boldsymbol{\theta}}[(\hat{\boldsymbol{\theta}}(\mathbf{y}) - \boldsymbol{\theta})^H(\hat{\boldsymbol{\theta}}(\mathbf{y}) - \boldsymbol{\theta})]. \quad (55)$$

Here, $\mathbb{E}_{\mathbf{y};\boldsymbol{\theta}}[\cdot]$ denotes the expectation taken with respect to the probability density function (pdf) $p(\mathbf{y};\boldsymbol{\theta})$ of the measurement vector \mathbf{y} parameterized by $\boldsymbol{\theta}$. A commonly employed approach seeks unbiased estimators satisfying $\mathbb{E}_{\mathbf{y};\boldsymbol{\theta}}[\hat{\boldsymbol{\theta}}(\mathbf{y})] = \boldsymbol{\theta}$ which



(a) Scenario 1



(b) Scenario 2

Fig. 5. Normalized frequency MSE for Scenarios 1 and 2.

TABLE IV

THE PARTIAL DERIVATIVES OF $\mathbf{s}(\mathbf{x})$ WITH RESPECT TO $\underline{\mathbf{x}}$. NOTE THAT \mathbf{e}_k IS A STANDARD BASIS VECTOR WITH A k TH COMPONENT OF ONE AND ALL THE OTHER COMPONENTS BEING ZERO

$k \& l \setminus \partial(\cdot) / \partial(\cdot)$	$\frac{\partial \mathbf{s}}{\partial \mathbf{x}_k}$	$\frac{\partial \mathbf{s}}{\partial \mathbf{x}_l}$	$\frac{\partial \mathbf{s}}{\partial \mathbf{x}_l^*}$	$\frac{\partial \mathbf{s}}{\partial \mathbf{x}_k^*}$
$K+1 \leq k \leq K+KT, K \leq l \leq K+KT$	$(\mathbf{I}_T \otimes \mathbf{A}) \mathbf{e}_{k-K}$	$(\mathbf{I}_T \otimes \mathbf{A}) \mathbf{e}_{l-K}$	$\mathbf{0}_{NT}$	$\mathbf{0}_{NT}$
$K+1 \leq k \leq K+KT, K+KT+1 \leq l \leq K+2KT$	$(\mathbf{I}_T \otimes \mathbf{A}) \mathbf{e}_{k-K}$	$\mathbf{0}_{NT}$	$(\mathbf{I}_T \otimes \mathbf{A}) \mathbf{e}_{l-K-KT}$	$\mathbf{0}_{NT}$
$K+KT+1 \leq k \leq K+2KT, K \leq l \leq K+KT$	$\mathbf{0}_{NT}$	$(\mathbf{I}_T \otimes \mathbf{A}) \mathbf{e}_{l-K}$	$\mathbf{0}_{NT}$	$(\mathbf{I}_T \otimes \mathbf{A}) \mathbf{e}_{k-K-KT}$
$K+KT+1 \leq k \leq K+2KT, K+KT+1 \leq l \leq K+2KT$	$\mathbf{0}_{NT}$	$\mathbf{0}_{NT}$	$(\mathbf{I}_T \otimes \mathbf{A}) \mathbf{e}_{l-K-KT}$	$(\mathbf{I}_T \otimes \mathbf{A}) \mathbf{e}_{k-K-KT}$

minimize MSE. Fortunately, the performance of an unbiased estimator can be characterised by the CRB. In the AWGN scenario, to evaluate the CRB for model (1) in the case of $\Phi = \mathbf{I}$, the following lemma is utilized.

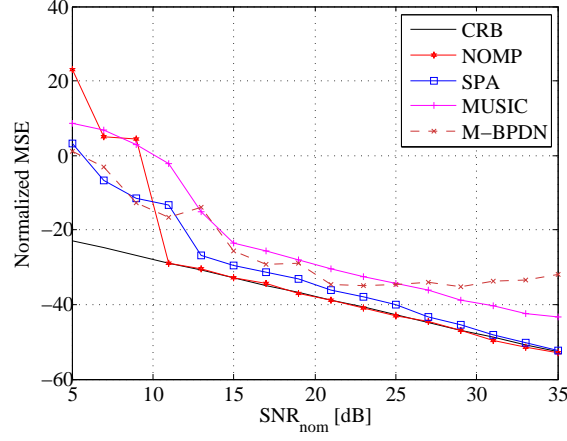
Lemma 2 [27] (*General Complex Gaussian CRLB*) Assume the observations \mathbf{y} follow the complex Gaussian distribution $\mathbf{y} \sim \mathcal{CN}(\mathbf{s}(\boldsymbol{\theta}), \Gamma(\boldsymbol{\theta}))$, then the (k, l) th element of the complex FIM $\mathbf{J}(\boldsymbol{\theta})$ is

$$[\mathbf{J}(\boldsymbol{\theta})]_{kl} = \left[\frac{\partial \mathbf{s}}{\partial \boldsymbol{\theta}_k} \right]^H \Gamma^{-1}(\boldsymbol{\theta}) \left[\frac{\partial \mathbf{s}}{\partial \boldsymbol{\theta}_l} \right] + \left[\frac{\partial \mathbf{s}}{\partial \boldsymbol{\theta}_l^*} \right]^H \Gamma^{-1}(\boldsymbol{\theta}) \left[\frac{\partial \mathbf{s}}{\partial \boldsymbol{\theta}_k^*} \right] + \text{tr} \left\{ \left[\frac{\partial \Gamma}{\partial \boldsymbol{\theta}_k^*} \right] \Gamma^{-1}(\boldsymbol{\theta}) \left[\frac{\partial \Gamma}{\partial \boldsymbol{\theta}_l} \right] \Gamma^{-1}(\boldsymbol{\theta}) \right\}, \quad (56)$$

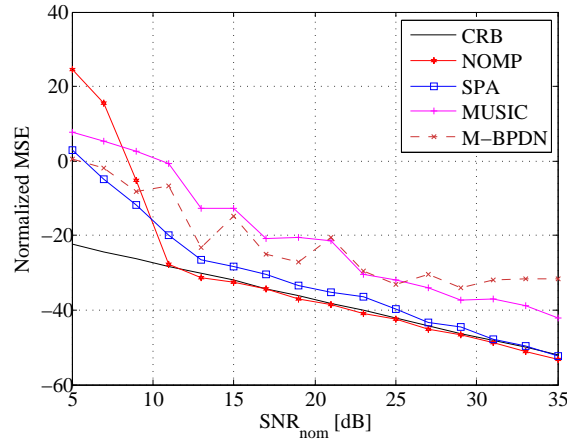
where $\boldsymbol{\theta} = [\boldsymbol{\theta}^T, \boldsymbol{\theta}^H]^T \in \mathbb{C}^{2p}$.

By vectorizing both sides of model (1), we can obtain

$$\mathbf{y} = (\mathbf{I}_T \otimes \mathbf{A}) \mathbf{x} + \mathbf{z}, \quad (57)$$



(a) Scenario 3



(b) Scenario 4

Fig. 6. Normalized frequency MSE for Scenarios 3 and 4.

where $\mathbf{y} = \text{vec}(\mathbf{Y})$, $\mathbf{x} = \text{vec}(\mathbf{X})$, $\mathbf{z} = \text{vec}(\mathbf{Z})$. In this case, $\boldsymbol{\theta} = [\boldsymbol{\omega}^T, \underline{\mathbf{x}}^T]^T$, $\underline{\mathbf{x}} = [\mathbf{x}^T, \mathbf{x}^H]^T$ and $\boldsymbol{\omega} = [\omega_1, \omega_2, \dots, \omega_K]^T$. We can conclude that $\mathbf{s}(\boldsymbol{\theta}) = (\mathbf{I}_T \otimes \mathbf{A}) \mathbf{x}$, $\boldsymbol{\Gamma}(\boldsymbol{\theta}) = \sigma^2 \mathbf{I}_{NT}$. We divide the calculation of FIM into four parts,

$$\mathbf{J} = \begin{pmatrix} \mathbf{J}_{11} & \mathbf{J}_{12} \\ \mathbf{J}_{21} & \mathbf{J}_{22} \end{pmatrix}. \quad (58)$$

In the following, we calculate the submatrices of \mathbf{J} separately.

A. \mathbf{J}_{11}

The (k, l) th element of \mathbf{J} is

$$\begin{aligned} \mathbf{J}_{k,l} &= \left[\frac{\partial \mathbf{s}}{\partial \omega_k} \right]^H \boldsymbol{\Gamma}^{-1} \left[\frac{\partial \mathbf{s}}{\partial \omega_l} \right] + \left[\frac{\partial \mathbf{s}}{\partial \omega_l} \right]^H \boldsymbol{\Gamma}^{-1} \left[\frac{\partial \mathbf{s}}{\partial \omega_k} \right] = \frac{2}{\sigma^2} \mathcal{R} \left\{ \left[\left(\mathbf{I}_T \otimes \frac{\partial \mathbf{A}}{\partial \omega_k} \right) \mathbf{x} \right]^H \left[\left(\mathbf{I}_T \otimes \frac{\partial \mathbf{A}}{\partial \omega_l} \right) \mathbf{x} \right] \right\} \\ &\stackrel{(a)}{=} \frac{2}{\sigma^2} \mathcal{R} \left\{ \mathbf{x}^H \left[\mathbf{I}_T \otimes \left(\frac{\partial \mathbf{A}}{\partial \omega_k} \right)^H \right] \left(\mathbf{I}_T \otimes \frac{\partial \mathbf{A}}{\partial \omega_l} \right) \mathbf{x} \right\} \stackrel{(b)}{=} \frac{2}{\sigma^2} \mathcal{R} \left\{ \mathbf{x}^H \left[\mathbf{I}_T \otimes \left(\frac{\partial \mathbf{A}}{\partial \omega_k} \right)^H \frac{\partial \mathbf{A}}{\partial \omega_l} \right] \mathbf{x} \right\}, \end{aligned} \quad (59)$$

for $1 \leq k, l \leq K$, where equality (a) follows from $(\mathbf{A} \otimes \mathbf{B})^H = \mathbf{A}^H \otimes \mathbf{B}^H$, and (b) is a direct consequence of $(\mathbf{A} \otimes \mathbf{B})(\mathbf{C} \otimes \mathbf{D}) = (\mathbf{AC}) \otimes (\mathbf{BD})$. According to

$$\text{tr}(\mathbf{ABCD}) = \text{vec}^T(\mathbf{B}) [\mathbf{C} \otimes \mathbf{A}^T] \text{vec}(\mathbf{D}^T), \quad (60)$$

we can further write $\mathbf{J}_{k,l}$ as

$$\mathbf{J}_{k,l} = \frac{2}{\sigma^2} \mathcal{R} \left\{ \text{tr} \left[\left(\frac{\partial \mathbf{A}}{\partial \omega_l} \right)^T \left(\frac{\partial \mathbf{A}}{\partial \omega_k} \right)^* \mathbf{X}^* \mathbf{X}^T \right] \right\} \stackrel{(a)}{=} \frac{2}{\sigma^2} \mathcal{R} \left\{ \text{tr} \left[\left(\frac{\partial \mathbf{A}}{\partial \omega_l} \right)^H \frac{\partial \mathbf{A}}{\partial \omega_k} \mathbf{X} \mathbf{X}^H \right] \right\}, \quad (61)$$

where (a) follows from $\mathcal{R}(a + bj) = \mathcal{R}(a - bj)$. By defining

$$\mathbf{b}_l = \frac{\partial \mathbf{a}(\omega_l)}{\partial \omega_l}, \quad (62)$$

$$\Psi \triangleq \mathbf{X} \mathbf{X}^H \in \mathbb{C}^{K \times K}, \quad (63)$$

we obtain

$$\left(\frac{\partial \mathbf{A}}{\partial \omega_l} \right)^H \frac{\partial \mathbf{A}}{\partial \omega_k} = \begin{bmatrix} 0 & 0 & \frac{\partial \mathbf{a}(\omega_l)}{\partial \omega_l} & 0 & 0 \end{bmatrix}^H \begin{bmatrix} 0 & 0 & \frac{\partial \mathbf{a}(\omega_k)}{\partial \omega_k} & 0 & 0 \end{bmatrix} = \begin{bmatrix} 0 & 0 & \mathbf{b}_l & 0 & 0 \end{bmatrix}^H \begin{bmatrix} 0 & 0 & \mathbf{b}_k & 0 & 0 \end{bmatrix} = \begin{pmatrix} 0 & \cdots & 0 \\ \vdots & \mathbf{b}_l^H \mathbf{b}_k & \vdots \\ 0 & \cdots & 0 \end{pmatrix}_{K \times K}, \quad (64)$$

Thus

$$\mathbf{J}_{k,l} = \frac{2}{\sigma^2} \mathcal{R} \{ \mathbf{b}_l^H \mathbf{b}_k \Psi_{kl} \}, 1 \leq k, l \leq K. \quad (65)$$

B. \mathbf{J}_{22}

The (k, l) th element of \mathbf{J} is

$$\mathbf{J}_{22} = \frac{1}{\sigma^2} \begin{bmatrix} \mathbf{I}_T \otimes (\mathbf{A}^H \mathbf{A}) & \mathbf{0}_{KT \times KT} \\ \mathbf{0}_{KT \times KT} & \mathbf{I}_T \otimes (\mathbf{A}^H \mathbf{A}) \end{bmatrix} = \frac{1}{\sigma^2} \mathbf{I}_{2T} \otimes (\mathbf{A}^H \mathbf{A}). \quad (66)$$

for $K + 1 \leq k, l \leq K + 2KT$.

C. \mathbf{J}_{12}

The (k, l) th element of \mathbf{J} is

$$\begin{aligned} \mathbf{J}_{k,l} &= \begin{bmatrix} \frac{\partial \mathbf{s}}{\partial \omega_k} \end{bmatrix}^H \Gamma^{-1} \begin{bmatrix} \frac{\partial \mathbf{s}}{\partial x_l} \end{bmatrix} + \begin{bmatrix} \frac{\partial \mathbf{s}}{\partial x_l^*} \end{bmatrix}^H \Gamma^{-1} \begin{bmatrix} \frac{\partial \mathbf{s}}{\partial \omega_k} \end{bmatrix} = \begin{cases} \frac{1}{\sigma^2} \left[\left(\mathbf{I}_T \otimes \frac{\partial \mathbf{A}}{\partial \omega_k} \right) \mathbf{x} \right]^H (\mathbf{I}_T \otimes \mathbf{A}) \mathbf{e}_{l-K}, (a) \\ \frac{1}{\sigma^2} [(\mathbf{I}_T \otimes \mathbf{A}) \mathbf{e}_{l-K-KT}]^H \left(\mathbf{I}_T \otimes \frac{\partial \mathbf{A}}{\partial \omega_k} \right) \mathbf{x}, (b) \end{cases} \\ &= \begin{cases} \frac{1}{\sigma^2} \text{tr} \left\{ \mathbf{A}^T \left(\frac{\partial \mathbf{A}}{\partial \omega_k} \right)^* \mathbf{X}^* [\text{reshape}(\mathbf{e}_{l-K}, K, T)]^T \right\}, (a) \\ \frac{1}{\sigma^2} \text{tr} \left\{ \left(\frac{\partial \mathbf{A}}{\partial \omega_k} \right)^T \mathbf{A}^* \text{reshape}((\mathbf{e}_{l-K-KT})^*, K, T) \mathbf{X}^T \right\}, (b). \end{cases} = \begin{cases} \frac{1}{\sigma^2} \mathbf{a}_{i_1}^T \mathbf{b}_k^* \mathbf{X}_{k j_1}^*, (a) \\ \frac{1}{\sigma^2} \mathbf{b}_k^T \mathbf{a}_{i_2}^* \mathbf{X}_{j_2 k}, (b). \end{cases} \end{aligned} \quad (67)$$

where (a) is $1 \leq k \leq K$, $K + 1 \leq l \leq K + KT$, (b) is $1 \leq k \leq K$, $K + KT + 1 \leq l \leq K + 2KT$, $i_1 = \lfloor (l - K - 1)/T \rfloor + 1$, $j_1 = l - K - T(\lfloor (l - K - 1)/T \rfloor)$, $i_2 = l - K - KT - K(\lfloor (l - K - KT - 1)/K \rfloor)$, $j_2 = \lfloor (l - K - KT - 1)/K \rfloor + 1$.

D. \mathbf{J}_{21}

The (k, l) th element of \mathbf{J} is

$$\begin{aligned} \mathbf{J}_{k,l} &= \begin{bmatrix} \frac{\partial \mathbf{s}}{\partial x_k} \end{bmatrix}^H \Gamma^{-1} \begin{bmatrix} \frac{\partial \mathbf{s}}{\partial \omega_l} \end{bmatrix} + \begin{bmatrix} \frac{\partial \mathbf{s}}{\partial \omega_l} \end{bmatrix}^H \Gamma^{-1} \begin{bmatrix} \frac{\partial \mathbf{s}}{\partial x_k^*} \end{bmatrix} = \begin{cases} \frac{1}{\sigma^2} [(\mathbf{I}_T \otimes \mathbf{A}) \mathbf{e}_{k-K}]^H \left(\mathbf{I}_T \otimes \frac{\partial \mathbf{A}}{\partial \omega_l} \right) \mathbf{x}, (c) \\ \frac{1}{\sigma^2} \left[\left(\mathbf{I}_T \otimes \frac{\partial \mathbf{A}}{\partial \omega_l} \right) \mathbf{x} \right]^H (\mathbf{I}_T \otimes \mathbf{A}) \mathbf{e}_{k-K-KT}, (d), \end{cases} \\ &= \begin{cases} \frac{1}{\sigma^2} \text{tr} \left\{ \left(\frac{\partial \mathbf{A}}{\partial \omega_l} \right)^T \mathbf{A}^* \text{reshape}((\mathbf{e}_{k-K})^*, K, T) \mathbf{X}^T \right\}, (c) \\ \frac{1}{\sigma^2} \text{tr} \left\{ \mathbf{A}^T \left(\frac{\partial \mathbf{A}}{\partial \omega_l} \right)^* \mathbf{X}^* [\text{reshape}(\mathbf{e}_{k-K-KT}, K, T)]^T \right\}, (d). \end{cases} = \begin{cases} \frac{1}{\sigma^2} \mathbf{b}_l^T \mathbf{a}_{i_3}^* \mathbf{X}_{j_3 l}, (c) \\ \frac{1}{\sigma^2} \mathbf{a}_{i_4}^T \mathbf{b}_l^* \mathbf{X}_{l j_4}, (d) \end{cases} \end{aligned} \quad (68)$$

where (c) is $1 \leq l \leq K$, $K + 1 \leq k \leq K + KT$, (d) is $1 \leq l \leq K$, $K + KT + 1 \leq k \leq K + 2KT$, $i_3 = k - K - K(\lfloor (k - K - 1)/K \rfloor)$, $j_3 = \lfloor (k - K - 1)/K \rfloor + 1$, $i_4 = \lfloor (k - K - KT - 1)/T \rfloor + 1$, $j_4 = k - K - KT - T(\lfloor (k - K - KT - 1)/T \rfloor)$.

REFERENCES

- [1] H. V. Poor, An introduction to signal detection and estimation, Springer-Verlag New York, 1994.
- [2] S. M. Kay, *Fundamentals of Statistical Signal Processing, Volume I: Estimation Theory*, 1993, Englewood Cliffs, NJ: Prentice Hall.
- [3] R. Schmidt, "Multiple emitter location and signal parameter estimation," *IEEE Trans. Antennas Propag.*, vol. 34, no. 3, pp. 276-280, 1986.
- [4] R. Roy and T. Kailath, "ESPRIT - estimation of signal parameters via rotational invariance techniques," *IEEE Trans. Acoust., Speech, Signal Process.*, vol. 37, no. 7, pp. 984-995, 1989.
- [5] H. Teutsch, *Modal Array Signal Processing: Principles and Applications of Acoustic Wavefield Decomposition*, ser. Lecture Notes in Control and Information Sciences. Berlin, Germany: Springer, 2007
- [6] D. Malioutov, M. Cetin, and A. Willsky, "A sparse signal reconstruction perspective for source localization with sensor arrays," *IEEE Trans. Signal Process.*, vol. 53, no. 8, pp. 3010-2022, 2005.
- [7] M. Hyder and K. Mahata, "Direction-of-arrival estimation using a mixed $\ell_{2,0}$ norm approximation," *IEEE Trans. Signal Process.*, vol. 58, no. 9, pp. 4646-4655, 2010.
- [8] E. Candes and J. Romberg, "Sparsity and incoherence in compressive sampling," *Inverse problems*, vol. 23, no. 3, pp. 969, 2007.
- [9] Y. Chi, L. L. Scharf, A. Pezeshki, and R. Calderbank, "Sensitivity to basis mismatch in compressed sensing," *IEEE Trans. Signal Process.*, vol. 59, no. 5, pp. 2182-2195, 2011.
- [10] L. L. Scharf, E. K. Chong, A. Pezeshki, and J. R. Luo, "Sensitivity considerations in compressed sensing," in Proceedings of the Asilomar Conference on Signals, *Systems and Computers*. *IEEE*, pp. 744-748, 2011.
- [11] P. Pakrooh, L. L. Scharf, A. Pezeshki, and Y. Chi, "Analysis of fisher information and the Cramer-Rao bound for nonlinear parameter estimation after compressed sensing," *IEEE Trans. Signal Process.*, vol. 63, no. 23, pp. 6423-6428, Dec. 2015.
- [12] P. Stoica, P. Babu, and J. Li, "New method of sparse parameter estimation in separable models and its use for spectral analysis of irregularly sampled data," *IEEE Trans. Signal Process.*, vol. 59, no. 1, pp. 35-47, 2011.
- [13] P. Stoica, P. Babu, and J. Li, "SPICE: A sparse covariance-based estimation method for array processing," *IEEE Trans. Signal Process.*, vol. 59, no. 2, pp. 629-638, 2011.
- [14] P. Stoica and P. Babu, "SPICE and LIKES: Two hyperparameter-free methods for sparse-parameter estimation", *Signal Process.*, vol. 92, no. 7, pp. 1580-1590, 2012.
- [15] Z. Yang, L. Xie, and C. Zhang, "A discretization-free sparse and parametric approach for linear array signal processing," *IEEE Trans. Signal Process.*, vol. 62, no. 19, pp. 4959-4973, 2014.
- [16] Y. Li and Y. Chi, "Off-the-grid line spectrum denoising and estimation with multiple measurement vectors," *IEEE Trans. Signal Process.*, vol. 64, no. 5, pp. 1257-1269, 2015.
- [17] J. Fang, F. Wang, Y. Shen, H. Li, and R. S. Blum, "Super-resolution compressed sensing for line spectral estimation: an iterative reweighted approach," *IEEE Trans. Signal Process.*, vol. 64, no. 18, pp. 4649-4662, 2016.
- [18] B. Mamandipoor, D. Ramasamy, and U. Madhow, "Newtonized orthogonal matching pursuit: Frequency estimation over the continuum," *IEEE Trans. Signal Process.*, vol. 64, no. 19, pp. 5066-5081, 2016.
- [19] A. Hjørungnes, *Complex-Valued Matrix Derivatives: With Applications in Signal Processing and Communications*, Cambridge University Press, 2011.
- [20] A. Schaeffer, "Inequalities of a. markoff and s. bernstein for polynomials and related functions," *Bull. Amer. Math. Soc.*, vol. 47, pp. 565-579, 1941.
- [21] B. N. Bhaskar, G. Tang, and B. Recht, "Atomic norm denoising with applications to line spectral estimation," *IEEE Trans. Signal Process.*, vol. 61, no. 23, pp. 5987-5999, 2013.
- [22] A. R. Barron, A. Cohen, W. Dahmen, and R. A. Devore, "Approximation and learning by greedy algorithms," *Ann. Statist.*, pp. 64-94, 2008.
- [23] J. A. Tropp and A. C. Gilbert, "Signal recovery from random measurements via orthogonal matching pursuit," *IEEE Trans. Inf. Theory*, vol. 53, no. 12, pp. 4655-4666, 2007.
- [24] E. V. D. Berg and M. P. Friedlander, "Sparse optimization with least-squares constraints," *SIAM J. Optim.*, vol 21, no.4, pp. 1201-1229, 2011.
- [25] Z. Yang and L. Xie, "On gridless sparse methods for line spectral estimation from complete and incomplete data," *IEEE Trans. Signal Process.*, vol. 63, no. 12, pp. 3139-3153, 2015.
- [26] Z. Yang and L. Xie, "Exact joint sparse frequency recovery via optimization methods," *IEEE Trans. Signal Process.*, vol. 64, no. 19, pp. 5145-5157, Oct 1, 2016.
- [27] V. Nagesha and S. M. Kay, "Cramer-Rao lower bounds for complex parameters," available at www.ele.uri.edu/faculty/kay/New%20web/downloadable%20files/Nageha_complex%20CRLB.pdf.